Covalent inhibitors for eradication of drug-resistant HIV-1 reverse transcriptase: From design to protein crystallography

Albert H. Chan[a,b], Won-Gil Lee[c], Krasimir A. Spasov[a,b], José A. Cisneros[c], Shalley N. Kudalkar[a,b], Zaritza O. Petrova[a,b], Amanda B. Buckingham[a,b], Karen S. Anderson[a,b,1], and William L. Jorgensen[c,1]

[a]Department of Pharmacology, Yale University School of Medicine, New Haven, CT 06520-8066; [b]Department of Molecular Biophysics and Biochemistry, Yale University School of Medicine, New Haven, CT 06520-8066; and [c]Department of Chemistry, Yale University, New Haven, CT 06520-8107

Contributed by William L. Jorgensen, July 26, 2017 (sent for review June 26, 2017; reviewed by Maurizio Botta and Dennis C. Liotta)

Development of resistance remains a major challenge for drugs to treat HIV-1 infections, including those targeting the essential viral polymerase, HIV-1 reverse transcriptase (RT). Resistance associated with the Tyr181Cys mutation in HIV-1 RT has been a key roadblock in the discovery of nonnucleoside RT inhibitors (NNRTIs). It is the principal point mutation that arises from treatment of HIV-infected patients with nevirapine, the first-in-class drug still widely used, especially in developing countries. We report covalent inhibitors of Tyr181Cys RT (CRTIs) that can completely knock out activity of the resistant mutant and of the particularly challenging Lys103Asn/Tyr181Cys variant. Conclusive evidence for the covalent modification of Cys181 is provided from enzyme inhibition kinetics, mass spectrometry, protein crystallography, and antiviral activity in infected human T-cell assays. The CRTIs are also shown to be selective for Cys181 and have lower cytotoxicity than the approved NNRTI drugs efavirenz and rilpivirine.

HIV | reverse transcriptase | covalent inhibitors | X-ray crystallography | mass spectrometry

HIV-1 reverse transcriptase (RT) has been the primary molecular target for anti-HIV chemotherapy (1). This is reflected in the success of the once-a-day medications Atripla and Complera, which consist of two nucleoside RT inhibitors (NRTIs), emtricitabine and tenofovir, and one nonnucleoside RT inhibitor (NNRTI), either efavirenz or rilpivirine (2) (Fig. 1). A serious clinical complication with the use of these drugs is the development of resistant strains of HIV-1 with mutations in RT (3, 4). For NNRTIs, the most common resistance mutations are Lys103Asn (K103N) and Tyr181Cys (Y181C), which are observed in 57% and 25% of patients failing NNRTI treatment (4). Y181C has been a major hurdle in the development of NNRTIs (1, 5, 6); it is debilitating for many NNRTIs, including the first approved drug in this class, nevirapine. Nevertheless, nevirapine remains on the WHO's Model List of Essential Medicines and it is used in the developing world as a monotherapy to prevent mother-to-child viral transmission. Furthermore, the double variant K103N/Y181C negates the efficacy of almost all NNRTIs except the most recently introduced etravirine and rilpivirine (4, 7).

In this report, we present a strategy for combating and possibly eradicating variant HIV-1 strains containing Y181C, including K103N/Y181C. Specifically, we report covalent HIV-1 RT inhibitors (CRTIs) that modify Cys181 and that yield complete inactivation of Cys181-containing HIV-1 RT. The work starts from our prior report of NNRTIs in the 2-naphthyl class of catechol diethers (8). In particular, a feature of the crystal structure of compound **1** (8) bound to wild-type RT caught our attention (Fig. 2). The carbon–chlorine bond is oriented toward Tyr181 in such a manner as to suggest that its replacement with an electrophilic warhead could result in covalent modification of Cys181 variants. For successful irreversible covalent inhibition, the inhibitor is expected to first bind to the target protein, then form the covalent bond (9, 10). The addition of a warhead would add steric bulk in the vicinity of the chlorine atom in Fig. 2; however, accommodation of reasonably sized groups was expected since we had observed nanomolar activity in standard infected T-cell assays for analogs of **1** with the chlorine replaced by groups as large as ethoxy, isopropyl, and cyclopropylmethyl (8). Then, to avoid off-target covalent inhibition, warheads of relatively low activity toward cysteine were desired, so α-halo ketones, α-halo amides, and acrylamides emerged as candidates (11). In view of the anticipated separation of the thiol group of Cys181 and the warheads, attention focused on the latter two options, specifically in compounds **2**–**5** (Fig. 3). It was further expected that secondary amides would be less likely to be successful than tertiary amides since an *E*-amide conformation, as indicated in **4**, would be needed to direct the vinyl group toward Cys181. Secondary *E*-amides are higher in energy by approximately 2.5 kcal/mol than the *Z* conformers, leading to an added reorganization penalty (12). A greater dehydration penalty could also be expected for secondary amides versus tertiary ones upon complex formation.

As reported here, compounds **2**–**5** were synthesized, and **3** and **5** are demonstrated to be covalent inhibitors of both Y181C and K103N/Y181C HIV-1 RT through in vitro and cell assays, mass spectrometry, and protein crystallography. This is a successful application of a covalent inhibition strategy to HIV-1 RT. Previous efforts also targeting Cys181, which explored analogs of MKC442

Significance

HIV-1 reverse transcriptase (RT) has been the prime target for anti-HIV chemotherapy; however, its rapid mutation often generates drug resistance. Prominent variant strains of HIV-1 that lead to treatment failure with nonnucleoside RT inhibitors (NNRTIs) bear the Tyr181Cys mutation in RT. Based on our previous discovery and crystallography for potent noncovalent NNRTIs, new compounds were designed with incorporation of chemical warheads intended to modify covalently Cys181. Here we report on the success of the strategy, including biochemical, biophysical, and cellular evidence of the desired irreversible covalent inhibition. The new compounds completely eliminate the activity of Cys181-bearing RT, and it may be possible to dose them less frequently than noncovalent inhibitors.

Author contributions: K.S.A. and W.L.J. designed research; A.H.C., W.-G.L., K.A.S., J.A.C., S.N.K., Z.O.P., A.B.B., and W.L.J. performed research; A.H.C., W.-G.L., K.A.S., J.A.C., S.N.K., Z.O.P., A.B.B., K.S.A., and W.L.J. analyzed data; and A.H.C., K.S.A., and W.L.J. wrote the paper.

Reviewers: M.B., University of Siena; and D.C.L., Emory University.

The authors declare no conflict of interest.

Data deposition: The atomic coordinates and structure factors have been deposited in the Protein Data Bank, www.wwpdb.org (PDB ID codes 5VQQ, 5VQR, 5VQS, 5VQT, 5VQU, 5VQV, 5VQW, 5VQX, 5VQY, and 5VQZ).

[1]To whom correspondence may be addressed. Email: karen.anderson@yale.edu or william.jorgensen@yale.edu.

This article contains supporting information online at www.pnas.org/lookup/suppl/doi:10.1073/pnas.1711463114/-/DCSupplemental.

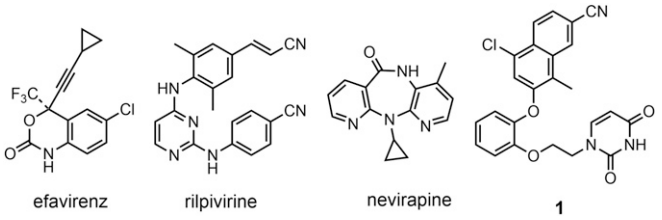

Fig. 1. Structures of NNRTIs.

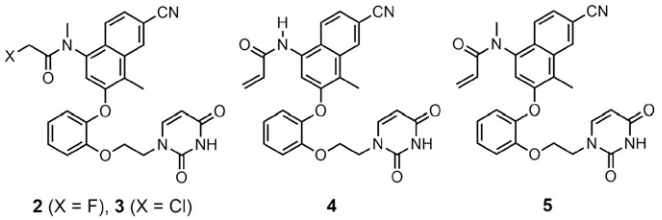

Fig. 3. Structures of potential covalent inhibitors of HIV-1 reverse transcriptase bearing the Y181C mutation.

(emivirine, a clinical candidate with Y181C resistance), were not fruitful (13, 14).

Results

Organic Synthesis. Preparation of **2**–**5** proceeded in a manner similar to that for other analogs of **1** (8) (Fig. 4). The starting points were previously reported 5-amino-7-(2-methoxyphenoxy)-8-methyl-2-naphthonitriles, which arose from Ullmann condensations (8). Acylation and unmasking of the hydroxyl group with BBr_3, followed by alkylation with N-Bz-protected 1-bromoethyluracil and deprotection delivered the desired compounds. Complete details on the preparation of the compounds along with the analytical data are provided in *SI Appendix*. The identity of assayed compounds was confirmed by ^1H and ^{13}C NMR, high-resolution mass spectrometry, and ultimately X-ray crystallography of complexes with RT; HPLC analyses established purity as >95%.

Activity Assays. Both in vitro and cell assays were undertaken. Wild-type (WT) and mutant forms (Y181C and K103N/Y181C) of the enzyme were tested as well as viral strains containing WT and the variant containing the K103N/Y181C mutations in RT. Execution of the enzymatic assays with different preincubation times for the inhibitors and RT readily indicated that covalent attachment to Cys181 was likely occurring with **3** and **5** and not with **2** and **4** (Table 1). As expected for noncovalent inhibition, the IC_{50} results in all four cases show little dependence on incubation time over 48 h for WT enzyme, which contains Tyr181. Similarly, for the Y181C and K103N/Y181C mutants there is little incubation-time dependence with **2** and **4**. However, as expected for covalent inhibitors (9), the activities of **3** and **5** show clear increases in potency (lower IC_{50} values) with increasing time for both variants containing Cys181. Over time, increasing amounts of the enzyme are inactivated in these cases. Furthermore, after 48 h, the IC_{50}s for **3** and **5** with the variants are significantly lower (0.14–0.19 μM) than their WT IC_{50}s (~1 μM), showing a near 10-fold increase in potency. This pattern is abnormal for noncovalent RT inhibitors.

Time-dependent inhibition kinetic analyses were also carried out with Y181C RT. The results for fraction activity for **3** and **5** as a function of concentration and incubation time are shown in Fig. 5*A*, while Fig. 5*B* contains the results for fraction activity with **2**–**5** extended to 75 h. The latter results are particularly striking, contrasting the constant lowered activity with the noncovalent inhibitors versus the steadily declining catalytic activity with **3** and **5**. After 3 d, there is essentially complete suppression of the activity of Y181C RT with acrylamide derivative **5**; the simple interpretation is that all of the enzyme has been irreversibly damaged by covalent modification of Cys181.

Values for the noncovalent binding constant of the inhibitors (K_i) and the rate constant of the subsequent covalent-bond-forming step (k_2) were also obtained for **3** and **5** using standard methods (9). The fractional activity (f) was measured at increasing inhibitor (I) concentrations as a function of incubation time t (*SI Appendix*, Fig. S1), which yields $-k_{obs}$ at each concentration from the slope of ln f versus t. k_{obs} is then plotted versus [I] as shown in Fig. 5*C* and fit to $k_{obs} = k_2\,[I]/(K_i + [I])$. The results, which are detailed in *SI Appendix*, Table S1, indicate values near 20 μM for K_i and a slightly faster k_2 for **5** ($4 \times 10^{-4}\cdot s^{-1}$) than for **3** ($3 \times 10^{-4}\cdot s^{-1}$). The crystal structures presented below suggest that the present inhibitors are larger than optimal, causing substantial expansion of the binding site. Future smaller designs may be able to increase the rate of deactivation by both increasing k_2 and lowering K_i. Utilization of more reactive warheads to increase k_2 can be expected to promote undesirable off-target activity.

Having established the time-dependent inhibition of activity with **3** and **5**, the next step was an evaluation of antiviral activity in HIV-1–infected cells. Wild-type and the drug resistant K103N/Y181C HIV-1 strains were chosen to assess anti-HIV activity at the cellular level. Results of the MT-2 assays using infected human T cells are shown in Table 2. In this case, standard assay conditions use an incubation time of 5 d to allow multiple rounds of viral replication, and the time is not varied (15, 16). The results for **1**, **2**, and **4** are typical for NNRTIs with the potency toward WT virus being greater than toward the double variant. However, **3** and **5** yield the unusual pattern in which the EC_{50} values for the WT virus and the K103N/Y181C variant are all similar, near 0.5 μM. With the noncovalent inhibitors, there is again an equilibrium established that impedes the viral replication; however, with the covalent inhibitors, virus bearing Y181C is increasingly debilitated as time progresses. It is

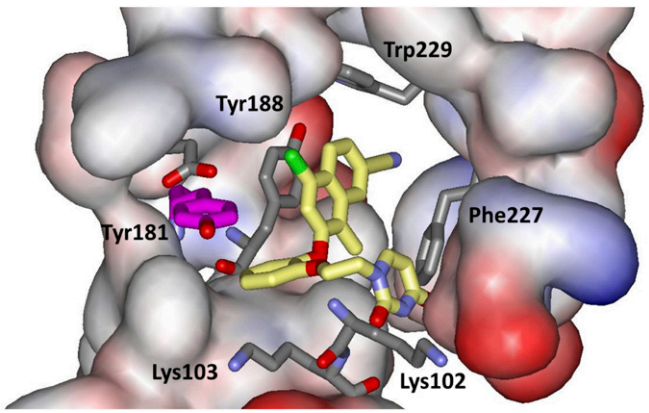

Fig. 2. Rendering from the 2.70-Å X-ray crystal structure (5TER) of **1** bound to WT HIV-1 reverse transcriptase. Carbon atoms for **1** and Tyr181 are in yellow and magenta, respectively.

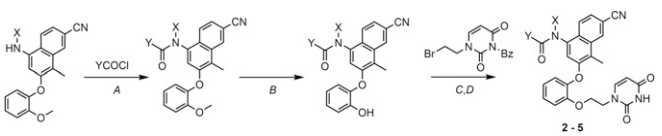

Fig. 4. General scheme for the syntheses of **2**–**5**. Reagents: (*A*) Et_3N, DCM, or THF, 0 °C to room temperature; (*B*) BBr_3, DCM, −78 °C to 0 °C, 3 h; (*C*) K_2CO_3, DMF, room temperature to 70 °C, 2 h; and (*D*) NH_4OH, DCM, 16 h.

Table 1. IC_{50} for wild-type and mutant RT after different preincubation times

Compound	1 h	24 h	48 h
		WT (μM)	
2	1.7 ± 0.2	5.3 ± 1.0	3.7 ± 1.7
3	2.1 ± 0.3	1.8 ± 0.2	1.1 ± 0.1
4	1.1 ± 0.1	2.0 ± 0.3	1.8 ± 0.2
5	1.1 ± 0.1	1.2 ± 0.2	1.4 ± 0.1
		Y181C (μM)	
2	4.1 ± 1.0	7.8 ± 2.5	5.0 ± 0.1
3	4.0 ± 1.3	0.48 ± 0.03	0.19 ± 0.02
4	2.4 ± 0.4	2.0 ± 0.4	3.8 ± 0.6
5	1.1 ± 0.2	0.40 ± 0.04	0.14 ± 0.04
		K103N/Y181C (μM)	
2	2.2 ± 0.2	5.7 ± 0.3	5.3 ± 0.4
3	1.4 ± 0.3	0.41 ± 0.07	0.19 ± 0.07
4	2.9 ± 0.2	7.2 ± 0.2	6.8 ± 0.5
5	2.6 ± 0.1	0.51 ± 0.05	0.18 ± 0.02

± indicates SD from triplicate measurements.

also important to note that the 50% cytotoxic concentration (CC_{50}) values of 32 μM for **3** and **5** are typical for this class of NNRTIs and higher than for efavirenz (15 μM) or rilpivirine (8 μM) (8). Thus, no enhanced T-cell cytotoxicity is apparent for the covalent inhibitors **3** and **5**.

Mass Spectrometry. Complexes of **2**–**5** with Y181C HIV-1 RT were studied by electrospray ionization-time of flight mass spectrometry (ESI-TOF MS) to determine the molecular weight of the intact protein and examine potential covalent modification reflected by an increase in mass. The results shown in Fig. 6 are consistent with the formation of covalent complexes when Y181C RT is incubated with **3** or **5**. A reference sample of Y181C RT showed peaks at 51,266 and 65,461 Da corresponding to the p51 and p66 subunits of RT. As p66 is the catalytic subunit containing the NNRTI binding site, only a modification of this subunit would be expected. For the noncovalent inhibitors **2** and **4**, these peaks remain in the same position within 5 Da mass precision. However, the p66 peak is shifted to approximately 65,956 Da for the covalent inhibitors **3** and **5**. The shifts of approximately 495 Da are fully consistent with the covalent modification of Cys181 in the p66 subunit by **3** and **5**, which would add masses of 482.5 and 496.5 Da, respectively. The presence of just a single shifted peak indicates that the covalent modification has occurred on only one residue.

Protein Crystallography. We have previously reported numerous crystal structures for complexes of NNRTIs with WT HIV-1 and variants from X-ray diffraction (8, 17, 18). As further described in *Materials and Methods*, the same procedures were used to obtain 10 structures that are reported here for WT RT with **2**–**5**, Y181C RT with **2**–**5**, and K103N/Y181C RT with **3** and **5** (*SI Appendix*, Figs. S2–S4). The resolution of the structures ranges from 2.2 to 2.6 -Å, and all 10 structures have been deposited in the Protein Data Bank. The structures fully support the assignment of **2** and **4** as noncovalent NNRTIs for all RT variants, and of **3** and **5** as CRTIs for Y181C and K103N/Y181C RT. For example, C–S single bonds between **3** and **5** and Cys181 are present in the structures for the complexes with Y181C RT in Fig. 7; the C–S bond lengths are both 1.82 Å. The corresponding structures for **3** and **5** with K103N/Y181C RT are essentially identical to those illustrated in Fig. 7, except near the K103N change. It may also be noted that the amide group in the linker in both cases has the methyl group *cis* to the carbonyl oxygen. As noted above, for the secondary amide **4**, the corresponding *E* conformation is destabilized, and the crystal structures for **4** with both WT and Y181C RT have the amide in the *Z* form. In these structures the vinyl group is directed more toward Pro95, there is a hydrogen bond (3.38 Å) between the amide carbonyl oxygen atom and the Cys181 sulfur, and the terminal vinyl carbon atom and the sulfur are separated by 3.90 Å. Another interaction to note is a hydrogen bond with O–N separations of 2.74 and 2.85 Å between a uracilyl oxygen atom of **3** and **5** and the backbone nitrogen of Lys103 in both structures in Fig. 7 and in Fig. 1.

The overall positioning of the new inhibitors is as expected from Fig. 1, although there are substantial adjustments. For example, the structures for **1** (8) and **5** with WT RT are compared in Fig. 8. There is an ~1.2-Å shift for **5** compared with **1** toward the back in Fig. 8, away from Tyr181. Notably, the side chain of Tyr188 rotates away from Trp229, such that the hydroxyl O to indolyl N distance

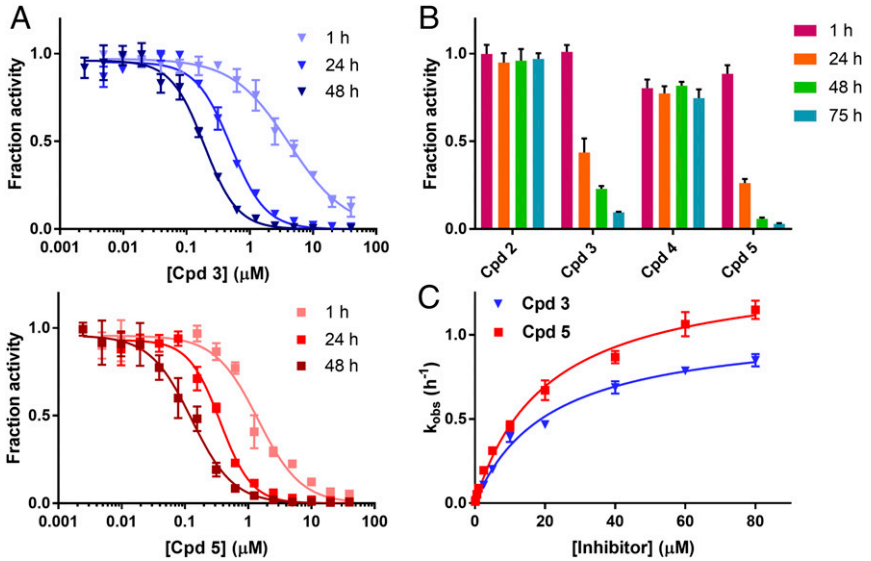

Fig. 5. Inhibition of Y181C RT activity in vitro. (*A*) IC_{50} curves of **3** (*Top*) and **5** (*Bottom*) after preincubating the enzyme and inhibitor for 1, 24, or 48 h. (*B*) Residual enzymatic activity after preincubating with 0.6 μM inhibitor for 1, 24, 48, or 75 h. At each time point, activity was normalized against a DMSO preincubation control. (*C*) k_{obs} as a function of inhibitor concentration used to obtain k_2 and K_i. All experiments were done in triplicate. Error bars represent SD.

Table 2. EC_{50} (μM) for HIV-1 and CC_{50} (μM) in MT-2 cell assays

	WT	K103N/Y181C	
Compound	EC_{50}	EC_{50}	CC_{50}
1*	0.0062	0.280	>100
2	0.890	15	>100
3	0.580	0.570	32
4	1.6	>12	11
5	0.560	0.500	32

*Results from ref. 8.

increases from 3.39 Å for **1** to 6.18 Å for **5**. This opens up space between Tyr181 and Tyr188 for accommodation of the acrylamide fragment of **5**. Concomitantly, both the textbook perpendicular edge-to-face aryl–aryl interaction between the naphthyl group of **1** and Trp229 and the parallel face-to-face interaction between **1** and Tyr188 become significantly canted for **5**. These distortions and a likely dehydration penalty for the amide carbonyl group of **5** undoubtedly contribute to the much weaker activity of **5** than **1** in the WT cell assay (Table 2). The same distortions are apparent in the structures for **3** and **5** with Y181C RT in Fig. 7 with even greater canting of the naphthyl group; the Tyr188 O to Trp229 indolyl N distances increase to 6.83 and 6.74 Å for **3** and **5**. It may also be noted that the other two cysteines in these structures, Cys38A in p66 and Cys38B in p51, are well resolved and they are not covalently modified.

Discussion

The Tyr181Cys (Y181C) mutation has been notorious in the history of the development of nonnucleoside inhibitors of HIV-1 reverse transcriptase. It arises early and yields full resistance in treatments of the virus with first-generation NNRTIs including nevirapine, delavirdine, 1-(2-2-hydroxyethoxymethyl)-6-(phenylthio)thymine (HEPT) analogs such as emivirine, and tetrahydroimidazo[4,5,1-jkj][1,4]benzodiazepin-2(1H)-one (TIBOs) (1–4). In combination with other mutations, especially Lys103Asn, it also yields virus resistant to a wide range of more recent NNRTIs, including efavirenz. For the present study, it was decided to pursue inhibitors that would covalently modify Cys181, and not just reduce, but rather destroy the activity of HIV-1 variants with Cys181. The therapeutic potential of such CRTIs needs careful evaluation. A simple application would be as adjuvants to prolong the efficacy of Y181C-sensitive NNRTIs. It may also be possible to discover a compound that has good noncovalent potency toward many viral variants and that reacts covalently with those bearing Y181C. Exploration of CRTIs that target other nucleophilic residues in RT is another possibility.

Toward these goals, initial results were reported for four potential CRTIs that arose from consideration of the crystal structure for the 2-naphthyl catechol diether **1** bound to wild-type HIV-1 RT (Fig. 1). Four different, mildly active warheads were incorporated in **2**–**5** that could react with the thiol group of Cys181. Success was obtained for the chloromethylamide **3** and the acrylamide **5**. The complete elimination of enzymatic activity over 3 d in Fig. 5*B* with the covalent inhibitors at submicromolar concentration is striking, in comparison with the steady state that is achieved with noncovalent NNRTIs. The mass spectrometric and crystallographic results confirm that Cys181 is selectively alkylated by the CRTIs, and the T-cell assay results revealed midnanomolar potency with no enhanced cytotoxicity for the CRTIs in comparison with typical NNRTIs.

The reported kinetic data and crystal structures provide guidance toward the generation of additional CRTIs with enhanced activity. In comparison with related noncovalent structures as in Fig. 1, it is apparent that the present CRTIs introduce increased strain and poorer aryl–aryl interactions in formation of the covalent complexes. Further efforts are focusing on compounds that, while maintaining selectivity, introduce less strain upon binding and reaction with Cys181.

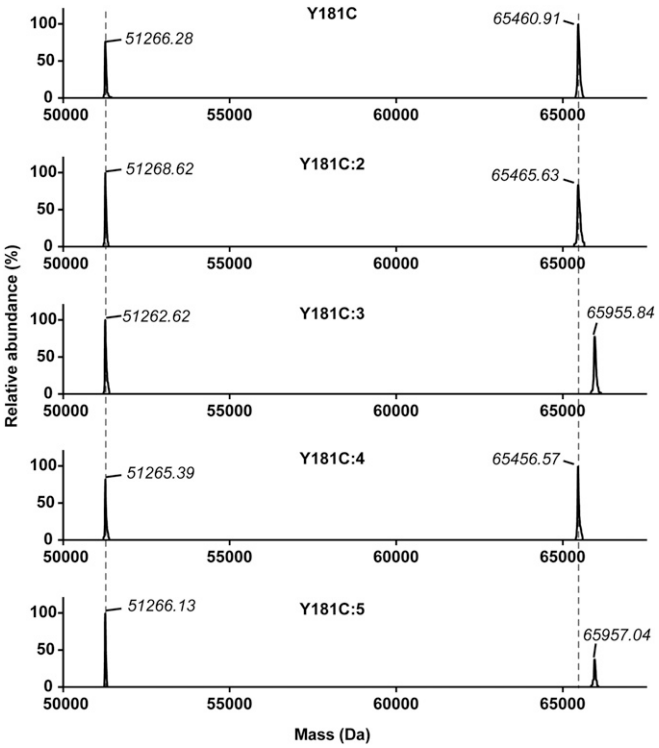

Fig. 6. ESI-TOF results for Y181C RT without and with inhibitors **2**–**5**. Dotted lines indicate the positions of p51 and p66 subunits in the Y181C only control.

Materials and Methods

Preparation of Compounds 2–5. Full synthetic details and characterization data are provided in *SI Appendix*.

Enzymatic Inhibition Assays. Recombinant wild-type and mutant HIV RT enzymes (p66/p51 heterodimer) were expressed and purified as previously described (19), and the concentration of active enzyme was determined by active site titration (17). A PicoGreen-based EnzChek Reverse Transcriptase Assay Kit (E22064; Thermo Fisher Scientific, Inc.) was used to determine RT activity in the presence of inhibitors, as reported previously (17). Briefly, in a 96-well plate, 5 μL of 100 nM active RT (in 50 mM imidazole pH 6.5, 50 mM NaCl, 10%

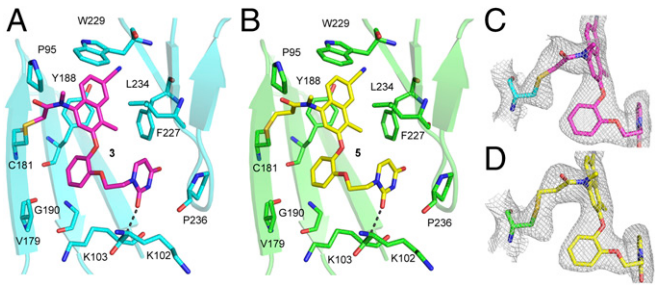

Fig. 7. Crystal structures of Y181C RT in complex with **3** and **5**. (*A*) Stick representation of the NNRTI binding pocket in the Y181C:**3** complex. The **3** forms a covalent bond with the thiol group of Cys181. A hydrogen bond with the backbone of Lys103 is indicated by the dotted line. (*B*) Same as *A* but with Y181C:**5**. (*C*) Electron density map (omit map contoured at 1.0 σ) around **3** and Cys181 showing continuous density between Cys181 and the inhibitor. (*D*) Same as *C* but with Y181C:**5**.

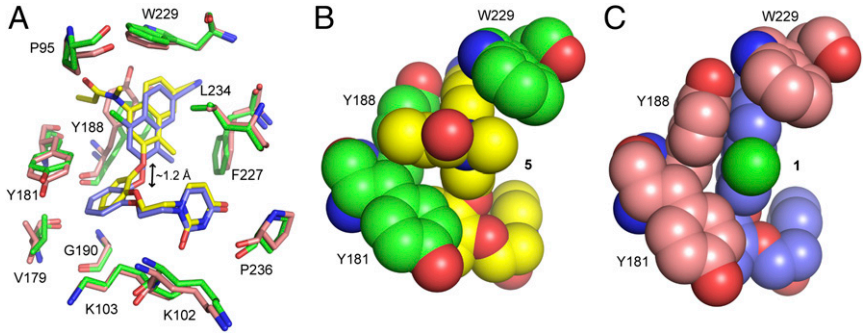

Fig. 8. Comparison of WT RT in complex with **1** and **5**. (*A*) Overlay of WT RT:**5** (**5** in yellow; protein in green) and WT RT:**1** (**1** in lilac; protein in pink) (PDB code 5TER). There is an ∼1.2-Å shift for the naphthyl and central phenyl rings. (*B*) Space filling model of WT RT:**5** showing the interaction of **5** with Y181, Y188, and W229. (*C*) Same as *B* but with WT RT:**1**. Note the tighter packing of Y188, **1**, and W229.

glycerol; final concentration in reaction was 20 nM) was preincubated with 1 μL of test compound or DMSO (control) at room temperature. After a set preincubation time, 20 μL of substrate solution [2.5 μg/mL $r(A)_{350}$ template, 0.125 μg/mL $d(T)_{16}$ primer in 60 mM Tris pH 8.1, 60 mM KCl, 8 mM $MgCl_2$, 13 mM DTT, 100 μM dTTP] was added to the enzyme-inhibitor solution to start the reaction. After 30 min of incubation at room temperature, 75 μL of 5 mM EDTA was added to quench the reaction. A total of 100 μL of 2× PicoGreen reagent was then added to each reaction and product formation was measured by a SpectraMax M5 plate reader (Molecular Devices) using excitation/emission = 485/520 nm. All samples were run in triplicate and the fluorescence readouts were normalized to DMSO controls to measure fraction activity.

Cell-Based Inhibition Assay. The procedures for the human MT-2 T-cell assays have been described in detail (8, 15, 16). Triplicate assays using the IIIB and the variant strain of HIV-1 (K103N/Y181C) were performed yielding EC_{50} values as the dose required to achieve 50% protection of the infected MT-2 cells as well as CC_{50} values for inhibition of MT-2 cell growth by 50%.

Mass Spectrometry. ESI-TOF MS was used to determine the molecular weight of complexes of **2–5** with Y181C HIV-1 RT. A total of 20 μM Y181C RT was incubated with 0.5 mM inhibitor in 1.25% DMSO or 1.25% DMSO alone overnight at room temperature. Before MS analyses, the samples were desalted by injecting 100-μL aliquots into a reverse-phase HPLC C4 column (5 μm, 4.6 × 100 mm; BioBasic 4 LC; Thermo Fisher Scientific, Inc.). Protein was eluted with a linear gradient of 25–100% solvent B over 40 min using a flow rate of 0.75 mL/min (solvent A, water; solvent B, acetonitrile, both with 0.1% formic acid and 0.02% TFA). Peak fractions were pooled, diluted four times with water, and concentrated to 100 μL. The concentrated samples were then injected into an Ettan ESI-TOF mass spectrometer (Amersham Biosciences) operated in positive ion mode.

Protein Crystallography. Recombinant wild-type and mutant RT52A enzyme optimized for crystallization was expressed and purified to homogeneity using methods described previously (18, 20). Both cocrystallization and soaking methods were used to obtain crystals, as described previously (8). Briefly, hanging drop vaporization with a protein:well solution ratio of 1:1 was used to screen crystallization conditions. In cocrystallization trials, 20 mg/mL protein was incubated with 0.5 mM inhibitor on ice for 1 h before setting up the drops. To prepare apo crystals for inhibitor soaking, 10 mg/mL protein was used instead in conjunction with preseeding (adding apo crystal microseeds at the time of setting up the tray). In the end, the best diffracting crystals of WT RT:**4** complex were obtained from cocrystallization in 50 mM MES pH 6.0, 14% (wt/vol) PEG 8000, 100 mM ammonium sulfate, 15 mM magnesium sulfate, and 5 mM spermine. For the rest of the complexes, soaking methods resulted in the best diffracting crystals. Crystals prepared for soaking were initially grown in 50 mM imidazole pH 6.5 or 6.8 or Hepes pH 7.0, 16–20% (wt/vol) PEG 8000, 100 mM ammonium sulfate, 15 mM magnesium sulfate, and 5 mM spermine. The 0.5-mM (final concentration) inhibitor was then added to the drops containing large crystals and soaked overnight. For freezing, all crystals were transferred to a cryosolution containing 27% (vol/vol) ethylene glycol and 0.5 mM inhibitor and flash cooled with liquid nitrogen.

Crystals were initially screened at the Yale Macromolecular X-ray Core Facility. Diffraction data for the best crystals were collected at Advanced Photon Source on beam line 24-ID-E through NE-CAT, using wavelength 0.979 Å. High-resolution datasets for the best diffracting crystals were processed with HKL2000 (21) or XDS (22). Difference Fourier methods were used to calculate phases in Phenix Refine (23). For WT RT:**4**, a preexisting model for WT RT: NNRTI (PDB 4WEI) (24) was used as an initial model (with the ligand, water, and ion removed). For WT RT:**2** and Y181C RT:**4**, a preexisting model for WT RT:**1** (PDB 5TER) (8) was used as the initial model instead. For the rest of the complexes, the final refined model of WT RT:**2** was used as the initial model. The program Coot (25) was used for model building into the electron density. Structures were refined using Phenix (23) until acceptable R factors, geometry statistics (ideal rmsd for bonds and angles), and Ramachandran statistics (>97% favored, 0% outliers) were achieved. Iterative build, composite omit electron density maps were generated using Phenix Autobuild (26).

Data collection, diffraction, and refinement statistics are summarized in *SI Appendix*, Tables S2–S4. Omit maps around the NNRTI binding pocket are illustrated in *SI Appendix*, Figs. S2 and S4. All structure figures were prepared with PyMOL (27). Crystallography programs were compiled by SBGrid (28). Structure factors and atomic coordinates have been deposited in the Protein Data Bank (PDB ID codes 5VQQ, 5VQR, 5VQS, 5VQT, 5VQU, 5VQV, 5VQW, 5VQX, 5VQY, 5VQZ).

ACKNOWLEDGMENTS. Gratitude is expressed to the NIH (Grants AI44616, GM32136, and GM49551) for research support and for Fellowship Award AI122864 (to A.H.C.). Crystal screening was conducted in the Yale Macromolecular X-ray Core Facility (NIH Grant 1S10OD018007-01). This work is based upon research conducted at the Northeastern Collaborative Access Team beamlines, which are funded by the National Institute of General Medical Sciences (NIH) (Grant P41 GM103403). This research used resources of the Advanced Photon Source, a US Department of Energy (DOE) Office of Science User Facility operated for the DOE Office of Science by Argonne National Laboratory under Contract DE-AC02-06CH11357. This research also used resources of the National Synchrotron Light Source II, a DOE Office of Science User Facility operated for the DOE Office of Science by Brookhaven National Laboratory under Contract DE-SC0012704.

1. Gubernick SI, Félix N, Lee D, Xu JJ, Hamad B (2016) The HIV therapy market. *Nat Rev Drug Discov* 15:451–452.
2. Sebaaly JC, Kelley D (2017) Single-tablet regimens for the treatment of HIV-1 infection. *Ann Pharmacother* 51:332–344.
3. Iyidogan P, Anderson KS (2014) Current perspectives on HIV-1 antiretroviral drug resistance. *Viruses* 6:4095–4139.
4. de Béthune MP (2010) Non-nucleoside reverse transcriptase inhibitors (NNRTIs), their discovery, development, and use in the treatment of HIV-1 infection: A review of the last 20 years (1989–2009). *Antiviral Res* 85:75–90.
5. Jorgensen WL, et al. (2011) Efficient discovery of potent anti-HIV agents targeting the Tyr181Cys variant of HIV reverse transcriptase. *J Am Chem Soc* 133:15686–15696.
6. Bollini M, et al. (2013) Optimization of benzyloxazoles as non-nucleoside inhibitors of HIV-1 reverse transcriptase to enhance Y181C potency. *Bioorg Med Chem Lett* 23:1110–1113.
7. Janssen PA, et al. (2005) In search of a novel anti-HIV drug: Multidisciplinary coordination in the discovery of 4-[[4-[[4-[(1E)-2-cyanoethenyl]-2,6-dimethylphenyl] amino]-2- pyrimidinyl]amino]benzonitrile (R278474, rilpivirine). *J Med Chem* 48: 1901–1909.
8. Lee WG, Chan AH, Spasov KA, Anderson KS, Jorgensen WL (2016) Design, conformation, and crystallography of 2-naphthyl phenyl ethers as potent anti-HIV agents. *ACS Med Chem Lett* 7:1156–1160.
9. Singh J, Petter RC, Baillie TA, Whitty A (2011) The resurgence of covalent drugs. *Nat Rev Drug Discov* 10:307–317.
10. Baillie TA (2016) Targeted covalent inhibitors for drug design. *Angew Chem Int Ed Engl* 55:13408–13421.
11. Barf T, Kaptein A (2012) Irreversible protein kinase inhibitors: Balancing the benefits and risks. *J Med Chem* 55:6243–6262.

12. Jorgensen WL, Gao J (1988) Cis trans energy difference for the peptide-bond in the gas-phase and in aqueous-solution. *J Am Chem Soc* 110:4212–4216.
13. Petersen L, Jessen CH, Pedersen EB, Nielsen C (2003) Synthesis and evaluation of new potential HIV-1 non-nucleoside reverse transcriptase inhibitors. New analogues of MKC-442 containing Michael acceptors in the C-6 position. *Org Biomol Chem* 1:3541–3545.
14. Aly YL, Pedersen EB, La Colla P, Loddo R (2006) Synthesis and anti-HIV-1 activity of novel MKC-442 analogues containing alkenyl chains or reactive functionalities in the 6-benzyl group. *Monatsh Chem* 137:1557–1570.
15. Lin TS, et al. (1994) Antiviral activity of 2′,3′-dideoxy-beta-L-5-fluorocytidine (beta-L-FddC) and 2′,3′-dideoxy-beta-L-cytidine (beta-L-ddC) against hepatitis B virus and human immunodeficiency virus type 1 in vitro. *Biochem Pharmacol* 47:171–174.
16. Ray AS, Yang Z, Chu CK, Anderson KS (2002) Novel use of a guanosine prodrug approach to convert 2′,3′-didehydro-2′,3′-dideoxyguanosine into a viable antiviral agent. *Antimicrob Agents Chemother* 46:887–891.
17. Gray WT, et al. (2015) Potent inhibitors active against HIV reverse transcriptase with K101P, a mutation conferring rilpivirine resistance. *ACS Med Chem Lett* 6:1075–1079.
18. Frey KM, et al. (2015) Structure-based evaluation of non-nucleoside inhibitors with improved potency and solubility that target HIV reverse transcriptase variants. *J Med Chem* 58:2737–2745.
19. Basavapathruni A, et al. (2006) Modulation of human immunodeficiency virus type 1 synergistic inhibition by reverse transcriptase mutations. *Biochemistry* 45:7334–7340.
20. Das K, et al. (2008) High-resolution structures of HIV-1 reverse transcriptase/TMC278 complexes: Strategic flexibility explains potency against resistance mutations. *Proc Natl Acad Sci USA* 105:1466–1471.
21. Otwinowski Z, Minor W (1997) Processing of X-ray diffraction data collected in oscillation mode. *Methods Enzymol* 276:307–326.
22. Kabsch W (2010) Xds. *Acta Crystallogr D Biol Crystallogr* 66:125–132.
23. Adams PD, et al. (2010) PHENIX: A comprehensive Python-based system for macromolecular structure solution. *Acta Crystallogr D Biol Crystallogr* 66:213–221.
24. Lee WG, et al. (2014) Picomolar inhibitors of HIV-1 reverse transcriptase: Design and crystallography of naphthyl phenyl ethers. *ACS Med Chem Lett* 5:1259–1262.
25. Emsley P, Lohkamp B, Scott WG, Cowtan K (2010) Features and development of coot. *Acta Crystallogr D Biol Crystallogr* 66:486–501.
26. Terwilliger TC, et al. (2008) Iterative-build OMIT maps: Map improvement by iterative model building and refinement without model bias. *Acta Crystallogr D Biol Crystallogr* 64:515–524.
27. DeLano WL (2009) PyMOL molecular viewer: Updates and refinements. *Abstr Pap Am Chem Soc*, 238 (abstr).
28. Morin A, et al. (2013) Collaboration gets the most out of software. *Elife* 2:e01456.